Gas entrainment allowance level at free surface and gas dynamic behavior of sodium-cooled fast reactor

Akira Yamaguchi [a,*], Eisaku Tatsumi [a], Takashi Takata [a], Kei Ito [b], Hiroyuki Ohshima [b], Hideki Kamide [b], Jun Sakakibara [c]

[a] Osaka University, 2-1, Yamada, Suita, Osaka 565-0871, Japan
[b] Japan Atomic Energy Agency, 4002, Oarai, Ibaraki 311-1393, Japan
[c] University of Tsukuba, Tennoudai 1-1-1, Tsukuba, Ibaraki 305-8573, Japan

ARTICLE INFO

ABSTRACT

In a sodium-cooled fast reactor (SFR), inert gases exist in the primary coolant system either in a state of dissolved gas or free gas bubbles. The sources of the gas bubbles are entrainment and dissolution of the reactor cover gas (argon) at the vessel free surface and emission of the helium gas that is produced as a result of disintegration of B_4C control rod material. The gas in the primary system may cause disturbance in reactivity, nucleation site for boiling, etc. Therefore, it is a key issue from the design and safety viewpoint and the allowance level is necessary regarding the gas entrainment at the free surface and the gas bubble concentration in the primary system. In the present study, a gas entrainment allowance level at the free surface is discussed and rationalized for the Japanese SFR (JSFR) design. The influence of the gas entrainment is evaluated using the void fraction at the core inlet. Design criteria for the acceptable level of the gas entrainment and gas concentration are proposed in consideration of the background level of gasses in the coolant. For the purpose, a plant dynamics code VIBUL has been developed to apply to the JSFR design to evaluate the concentration distribution of the dissolved gas and the free gas bubble in the JSFR system. Using the plant dynamics code for the bubble behavior, the background level of the free gas (void fraction at the core inlet) has been obtained. Assuming that the total void fraction should be kept below 105% of the background level, a preliminary design allowance level of gas entrainment is proposed as the map in terms of the entrainment rate and the entrained bubble radius. Furthermore, the possibility of bubble removal and design requirement of the device is investigated to satisfy the allowance level. It is noted that the background level is already very low in comparison with the induced void reactivity by the void passing the reactor core.

© 2011 Elsevier B.V. All rights reserved.

1. Introduction

In the Japanese sodium-cooled fast reactor (JSFR) design (Ichimiya et al., 2003), the thermal output and the reactor vessel diameter are 4.9 times and 1.5 times, respectively, as much as that of the prototype reactor Monju. Consequently, the coolant velocity is larger than the precedent SFR designs and the flow stabilization of the free surface in the reactor vessel and the prevention of the cover gas entrainment are key issues in terms of the design and safety. Technological challenge is necessary to assure the design feasibility, i.e., optimizing the components design and their arrangement and thermal-hydraulics in the reactor vessel.

One of the key design and safety issues is to limit the inert gas concentration existing in the primary coolant system either in a state of dissolved gas or free gas bubbles. The sources of the gas bubbles are entrainment and dissolution of the reactor cover gas (argon) at the vessel free surface and emission of the helium gas that is produced as a result of disintegration of B_4C control rod material. As the coolant velocity increases and the control rods are used for longer period than ever to achieve economical advantage of the JSFR, we anticipate more possibilities of gas contents in the primary coolant. In other words, the existence of the gasses in the primary heat transport system is inevitable in the advanced design. On the other hand, accumulation of small gas bubbles at a stagnant location is less plausible because of higher coolant velocity in the heat transport system. A safety design guideline requires large gas bubbles are not produced resulting from small bubbles accumulation.

As the coolant circulates in the primary system, the gas bubbles dissolve in the liquid sodium and/or dissolved gasses appear as bubbles. Nucleation and detachment of bubbles on the surface of
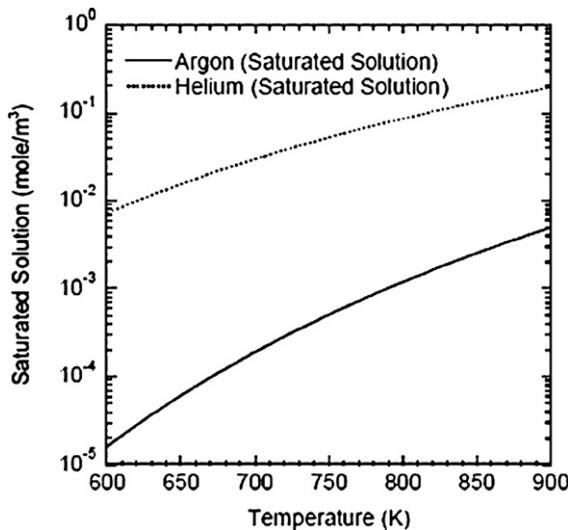
Fig. 1. Solubilities of argon and helium in sodium for the SFR operating temperature.

the heat transfer tubes in the intermediate heat exchanger (IHX) is an internal source of gas bubbles travelling to the reactor core. The dissolved gas appears by nucleation because the solubility of the gasses in sodium decreases as the temperature decreases as shown in Fig. 1. If the coolant temperature rises or the pressure increases, the bubbles tend to dissolve in the sodium. The gas in the primary system may cause disturbance in reactivity, nucleation site for boiling, etc. Therefore, it is one of the key issues from the design and safety viewpoint and the allowance level is needs to be established regarding the gas entrainment at the free surface and the gas bubble concentration in the primary system.

In order to predict the gas behavior in the heat transport system, a computational code VIBUL for one-dimensional plant dynamics of the gas in the primary system had been developed (Berton, 1991). The VIBUL code is based on multi-node flow network representation of the reactor vessel and the primary heat transport system. Simple models are used for various phenomena regarding gas behavior such as mass transfer, dissolution, bubble nucleation and detachment at the tube wall. In the present study, a parametric model for the gas behavior in the reactor plenum is derived based on multi-dimensional analysis in the upper plenum flow field and the gas bubble transportation. In addition, source term model of bubbles at the IHX is developed and is validated by comparing with experimental data. The VIBUL code is improved with the newly developed models and the prediction accuracy is enhanced to an extent.

The influence of the gas entrainment at the reactor free surface on the void fraction at the core inlet is estimated with the plant dynamics code. It is required to define the design allowance level of gas bubble concentration in the primary system. Design criteria for the acceptance of the gas entrainment and the gas concentration are proposed in consideration of the background level of the gasses in the coolant. Also investigated is the required performance of an apparatus that may be installed in the cold leg piping to remove the gas bubbles supposed to exist in the system.

2. Development of numerical method

2.1. Basic equation of gas dynamics and thermal hydraulics

The VIBUL code was originally developed for dynamics of gas behavior in a primary coolant system of a pool-type SFR (Berton, 1991) and modified by the authors for the loop-type JSFR design (Yamaguchi et al., 2005). The plant system is represented as a network consisting of volumes and paths. The volume expresses equipment or a part of the equipment such as a reactor upper plenum, an IHX, and pump. In the following, a volume is termed as a component. The bubble number density as a function of the bubble size and the total amount of the gas are estimated for every volume such as the hot plenum, the reactor core, and the IHX in the heat transport system. The bubble radius range is discretized in a logarithmic scale into groups between the minimum and the maximum radii. The representative radius of each group is expressed as:

$$r_i = r_{\min} \times 10^{k(i-1)}, \quad \text{where} \quad k = \frac{1}{K-1}\log_{10}\frac{r_{\max}}{r_{\min}}, \tag{1}$$

where r_i is the median radius of a bubble in class i, and $r_{\min}$ and $r_{\max}$ are the minimum and the maximum radii of the bubble size, respectively. The minimum and the maximum radii are determined so that the computational results are not sensitive to them. Let the number of the radius classes be K, the conservation of total mass of the gas in a component of the system is given by:

$$V_{\mathrm{Na}}\sum_{i=1}^{K}N_{bi}\frac{d}{dt}N_{mi} + V_{\mathrm{Na}}\frac{d}{dt}N_d$$
$$= -2\sqrt{\frac{Dv_hL}{\pi}}(N_d - H_cP_{FS}) - QN_d + Q\tilde{N}_d, \tag{2}$$

where N_b is the numbers of bubbles per unit volume in the component, N_m is the molar mass of the gas included in a bubble, N_d is the molar mass of the dissolved gas in a unit volume of sodium. V_{Na} is the volume of the component and Q is the volumetric flow rate of sodium. D, v_h, L, H_c and P_{FS} are the diffusion coefficient of the gas in the sodium (Clift et al., 1978), the horizontal velocity at the free surface, hydraulic diameter of the free surface, Henry's constant and the pressure of the cover gas, respectively. The free surface velocity is limited to be less than 0.2 m/s from the thermal hydraulic design requirement as 0.2 m/s. Henry's constant is defined as:

$$H_c = \frac{S\rho_{\mathrm{Na}}}{M_{\mathrm{Na}}} \tag{3}$$

where S is the solubility, ρ_{Na} is the sodium density and M_{Na} is the molar mass of sodium. The solubility for noble gases such as argon and helium are given by Reed and Dropher (1970). The first term in the right hand side of Eq. (2) expresses the diffusion terms at the free surface that appears only in a component with a free surface such as the upper plenum in the reactor vessel.

The conservation of the number of free gas bubbles in a component is expressed as Eq. (4) for the bubble size group i:

$$V_{\mathrm{Na}}\frac{d}{dt}N_{b,i} = -\alpha_i V_{\mathrm{Na}}N_{b,i} - QN_{b,i} + Q\tilde{N}_{b,i} + S_i \tag{4}$$

where N_b and $\tilde{N}_b$ are the numbers of bubbles per unit volume in the component and the sum of the inflow bubbles from the upstream paths, respectively. The bubble size group is designated as the subscript "i". The second and the third terms are advection effect by the outflow and the inflow. S_i is the source term of ith size radius. In the upper plenum of the reactor vessel, one considers the emission of the gas bubbles at the free surface and the source term by the gas entrainment. In the reactor core, there is another source term, i.e., emission of helium from the control rods. The first term in the right hand side of Eq. (4) represents the bubble emission at the free surface due to buoyancy. α_i is the degassing constant and is expressed as:

$$\alpha_i = \frac{S_{\mathrm{Na}}v_{t,i}}{V_{\mathrm{Na}}} \tag{5}$$

where S_{Na} is an area of the free surface, V_{Na} is a volume of the plenum and v_t is the terminal rising velocity of the bubble. The

degassing constant expresses the bubble emission rate per unit time.

A bubble is transported by a drag force and a buoyancy force, shrinking or growing according to the mass transfer between the gas phase and the liquid phase. The mass conservation equation for a single bubble is given by:

$$\frac{dN_{m,i}}{dt} = -4k_i\pi r_i^2 \left[H_c \left(P + \frac{2\sigma}{r_i} \right) - N_d \right] \tag{6}$$

where r is the radius of a bubble, P is the bulk pressure of the liquid sodium, and σ is the surface tension coefficient. k_i is a mass transfer coefficient which is given by:

$$k_i = \frac{\text{Sh}D}{2r_i} \tag{7}$$

where Sh is the Sherwood number.

Too large bubble breaks up in the components where the turbulence is significant. Such examples are the primary pump and the fuel subassemblies. Although the bubble break-up phenomenon in the components is not well understood, it is reasonable to consider a bubble break up due to the shear force caused by the velocity fluctuation (Lewis and Davidson, 1982). Let $\overline{u'^2}$ be the turbulent intensity and We_C be the critical Weber number, a critical bubble radius is evaluated as $r_C = \sigma \text{We}_C / 2\rho\overline{u'^2}$. It is assumed that a larger bubble than the critical radius split into two bubbles with the same diameters. The gas pressure of a very small bubble must increases significantly to balance the surface tension. Therefore, the small bubble is to dissolve instantaneously. In the previous study of the gas dynamics analysis (Yamaguchi et al., 2005), it was evaluated that most of the bubbles is in the range between 10 and 80 μm and the critical bubble radius is 250–300 μm.

2.2. Modeling of bubble behavior in reactor vessel

2.2.1. Parametric analysis of flow field in upper plenum

Important and key issue for predicting the gas bubble concentration in the SFR system is the modeling of the bubble source term and bubble sink term. The source terms are, as mentioned above, the gas entrainment, and the helium gas emission from the control rods. The sink term is the emission of the gas bubbles at the free surface. The helium gas emission is to be evaluated based on the design specification of reactor core and the control rods. It is preliminarily evaluated to be 2.4×10^{-7} m³/s (0.24 cc/s). The gas entrainment depends on the arrangement of the internal structures as well as the thermal hydraulic design. Authors will discuss on this point in the subsequent sections.

In the original VIBUL code, the gas behavior is simulated based on one point approximation. In the upper plenum, the flow field is complicated due to the internal structure and the core exit flow boundary conditions. Hence, the simplification is not sufficiently accurate to describe the gas behavior in the plenum where the multi-dimensional effect is dominant. With the one point model, bubbles emitted at the free surface is represented as the degassing constant as in Eq. (5). This approach assumes that the gas bubbles in a plenum are mixed uniformly and instantaneously. The sink term is evaluated with the degassing constant defined by Eq. (5) in the VIBUL code. The gas bubbles are rising at a constant terminal velocity and emitted from the free surface at the rate shown in Eq. (5). In addition, the residential time of bubbles in the plenum are constant irrespective to the bubble size and the flow pattern. It is noted that the definition is very simple and is evaluated using the representative size of the upper plenum (free surface area and volume) and the terminal velocity of bubbles. In addition, the dissolution of a gas bubble depends on the residential time and the size of the bubble in the upper plenum.
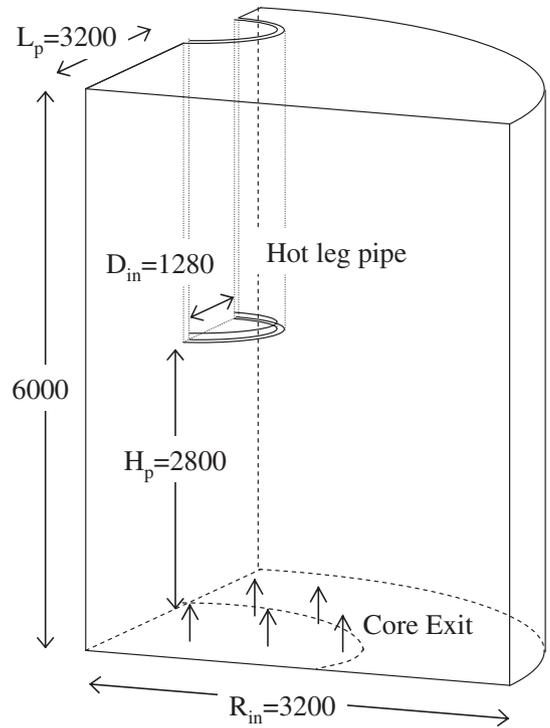

Fig. 2. Computational domain of reactor upper plenum.

The authors performed preliminary two-dimensional analyses and found that it is important to consider the geometry of the internals and the flow pattern of the reactor vessel for evaluating the degassing constant (Tatsumi et al., 2007). Then the authors perform a three dimensional analysis of the in-vessel coolant flow and bubble behavior to predicting the degassing constant more accurately based on the bubble transport characteristics and to develop correlation equations. And then we implement the model into the VIBUL code and compare the present model with the previous proposed two-dimensional model and one point approximation model. The simplified geometry of the reactor vessel model is shown in Fig. 2. One-fourth sector is modeled and the hot leg pipe is immersed in the liquid sodium. In the JSFR design, perforated plates are used as the above core structure and the core exit flow tends to go upward. Therefore the above core structure is not included in the three dimensional model in the present study.

Equations of mass and momentum conservation for a single bubble with radius r_i in a flow field are solved with the following equations.

$$\frac{d\boldsymbol{V}_G}{dt} = \boldsymbol{g} \left(\frac{\rho_L - \rho_G}{\rho_G} \right) + \frac{3}{8r}C_D \frac{\rho_L}{\rho_G} |\boldsymbol{V}_L - \boldsymbol{V}_G|(\boldsymbol{V}_L - \boldsymbol{V}_G) \tag{8}$$

$$\frac{dN_m}{dt} = -4k\pi r^2 [N'_d - N_d] \tag{9}$$

Accordingly, the gas behavior in the upper plenum is estimated using numerical simulation based on three-dimensional coordinates. Gas bubbles in the upper plenum either dissolve into liquid sodium, flowed out to hot leg pipe or emitted at the free surface. We define three variables regarding the mass fractions of the bubbles: released at the free surface (f_{rel}), dissolved in the liquid sodium (f_{dis}) and flowing out of the upper plenum (f_{out}). Three quantities sum up to unity.

Parameters of the three-dimensional analyses are the core exit average velocity V_{in}, the diameter of the hot leg pipe D_{out}, the elevation H_p and the radial location L_p of the hot leg pipe (see Fig. 2). Equally spaced mesh divided into $60 \times 60 \times 60$ is arranged to the computational region. The computational mesh
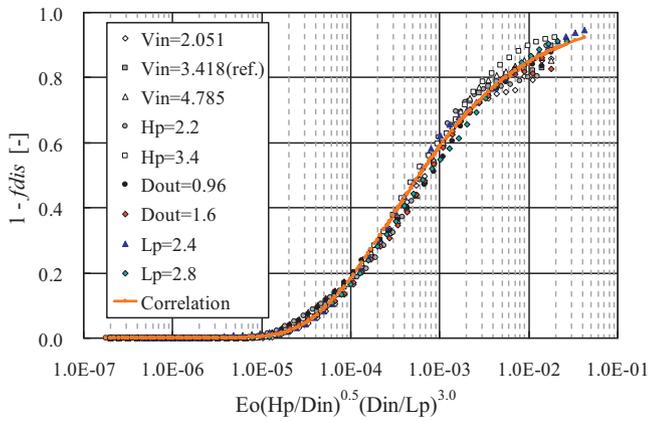
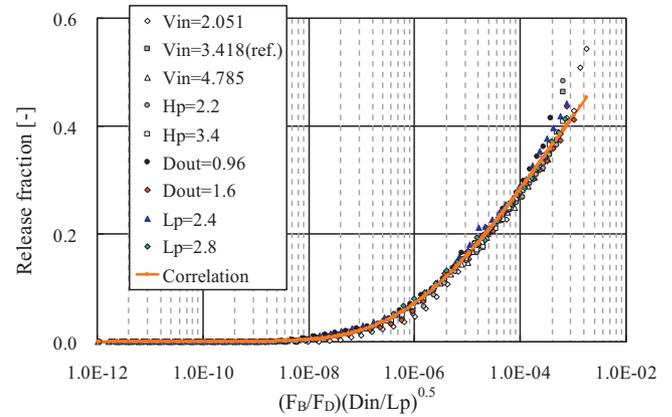Fig. 3. Non-dimensional expression of dissolved babble fraction.

Fig. 4. Non-dimensional expression of released babble fraction at free surface.

size is 0.08 m, 0.08 m and 0.1 m as Δx, Δy and Δz, respectively for the reference case. The velocity distribution at the core exit is based on the design value for inner core fuel assemblies, outer core fuel assemblies, blanket assemblies and shielding structures. Initial temperature in the upper plenum is 823 K. Although the dissolution of the bubble is related to the system pressure and initial molar concentration of the dissolved gas, atmospheric pressure and no initial dissolution are assumed for simplicity. Also, since the argon gas is the dominant source as shown in later (see Fig. 13), the helium gas is not considered. The details of the parametric analysis are given in Tatsumi (2008).

2.2.2. Correlations development for bubble behavior

We propose non-dimensional empirical correlations for gas behavior in the upper plenum based on the results of the parametric analyses. Some of the gas bubbles in the reactor vessel upper plenum dissolve in sodium. Others rise toward the free surface and are released into the cover gas. The rest of them flow out and discharged into the hot leg pipe. As shown in Eq. (6), the dissolution is related to the surface tension and the residence time. The surface tension is inversely proportional to the bubble radius. The residence time depends on the buoyancy and drag force. The buoyancy force and the drag force depend on the bubble diameter and the flow field, respectively. Therefore, dimensionless numbers to be considered should include surface tension, buoyancy and drag forces. In addition, non-dimensional lengths H_p/D_{in} and L_p/D_{in} are used to represent the relative location of the outlet nozzle in the upper plenum in terms of the pipe diameter. They are related to the dominance of the more stagnant circulating flow or the direct flow that reaches to the hot leg pipe. Here we introduce Eötvös number Eo that is the ratio of the buoyancy force and the surface tension as:

$$Eo = \frac{g(\rho_L - \rho_G)d^2}{\sigma} \tag{10}$$

where d is the bubble diameter. Ratio of the buoyancy force and the drag force, F_B/F_D, is written as:

$$\frac{F_B}{F_D} = \frac{8r\rho_G g}{3C_D((D_{in}/D_{out})V_{in})^2} \tag{11}$$

We plotted various cases of computations in Figs. 3 and 4 for f_{dis} and f_{rel}, respectively. Non-dimensional correlations for f_{dis} and f_{out} have been obtained as:

$$f_{dis} = 1.0 - \exp(-0.0161 \times X^{-0.5059}), \quad X = Eo \times \left(\frac{H_p}{D_{in}}\right)^{0.5} \left(\frac{D_{in}}{L_p}\right)^{3.0} \tag{12}$$

$$f_{rel} = \exp(-0.2953 \times X^{-0.1595}), \quad X = \left(\frac{F_B}{F_D}\right)\left(\frac{D_{in}}{L_p}\right)^{0.5} \tag{13}$$

where the correlation coefficients are quite high, that is larger than 0.98.

Eq. (12) suggests that the dissolution fraction depends on buoyancy and surface tension forces and the location of the outlet nozzle (H_p and L_p). On the other hand, from Eq. (13) the release fraction is dominated by buoyancy, and drag forces and the radial location of the outlet nozzle (L_p). The dissolution is dominant when bubbles are trapped and stay inside a circulation for long period. The release fraction increases as more bubbles are transported to the free surface. The release fraction from the free surface is determined by the fraction of the buoyancy force and the drag force as well as the relative dominance of the circulating flow and the direct flow. The fraction of bubbles flowing out of the nozzle, f_{out} is $1 - f_{dis} - f_{rel}$.

2.3. Bubble nucleation at IHX heat transfer tube

2.3.1. Gas bubble nucleation phenomenon

The temperatures in the hot and cold legs of the JSFR are 550 °C and 375 °C, respectively. Corresponding to the temperature change, the solubility varies by 10^{-1} mol/m³ for the argon gas and 10^{-3} mol/m³ as seen from Fig. 1. Therefore a gas bubble tends to dissolve and disappear in the reactor core where the sodium is heated up and dissolved gas tends to nucleate and turn to bubbles in the IHX. As the coolant flows along with the IHX heat transfer tubes, the temperature gradually decreases and it approaches to the saturation. At the location where the gas solubility equals the saturation solubility, the nucleation initiates. Beyond the location, gas bubbles emission continues to the end of the heat transfer tube, i.e., IHX outlet. If the bubbles grow large enough, the coolant flow detaches the bubbles and transports them downstream. It is the reason that the consideration of bubble existence in the primary coolant system is required. Needless to say, a gas bubble tends to dissolve and disappear in the reactor core where the sodium is heated up.

At the nucleation point where the dissolved gas concentration is saturated, the molar concentration is given by:

$$P_G = \frac{N_{de}}{H} \quad \text{where } H = \frac{S \times 10^{-5} \times \rho_{Na}}{M_{Na}}, \quad S = 10^{-2.13 - 4542/T} \tag{14}$$

according to the Henry's law using the molar concentration N_{de}, solubility S and the molar mass of sodium M_{Na}. As the differential pressure of bulk sodium pressure and bubble pressure ΔP equals the surface tension from the Laplace equation, the surface tension
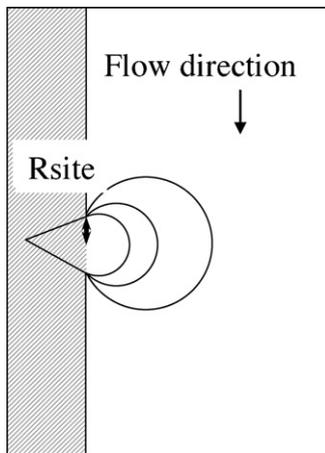
Fig. 5. Concept of the cavity radius.

Fig. 7. Force balance in crossflow direction.

is evaluated as:

$$\Delta P = \frac{2\sigma}{R_{site}} \tag{15}$$

where R_{site} is the cavity radius. Fig. 5 shows the concept of the cavity radius. A bubble nucleation takes place on the cavity with radius R_{site}. Subsequently, due to a mass transfer of the dissolved gas from the liquid sodium to the bubble, the bubble growth continues with the constant contact radius R_{site}.

As the initial bubble grows and becomes larger, the flow resistance increases. As a result, the bubble moves along with the tube in the flow direction. The bubble is subject to the following forces: surface tension with the tube wall, lift force with the sodium, and the growth force with the sodium. The growth force is the reacting force from the fluid when a bubble is growing. Force balance equations in the flow direction (Fig. 6) and the cross flow direction (Fig. 7) are given by:

$$\sum F_x = F_{sx} + F_{grx} + F_{sl} = \rho_g V_b \frac{dv_{gx}}{dt}, \quad \text{cross flow direction} \tag{16}$$

$$\sum F_y = F_{sy} + F_{gry} + F_B + F_D = \rho_g V_b \frac{dv_{gy}}{dt}, \quad \text{in flow direction} \tag{17}$$

where F_s, F_{gr}, F_{sl}, F_B, and F_D are forces acting on the bubble due to surface tension, bubble growth, lift, buoyancy, and drag, respectively. Here we assume the model proposed and validated by Situ
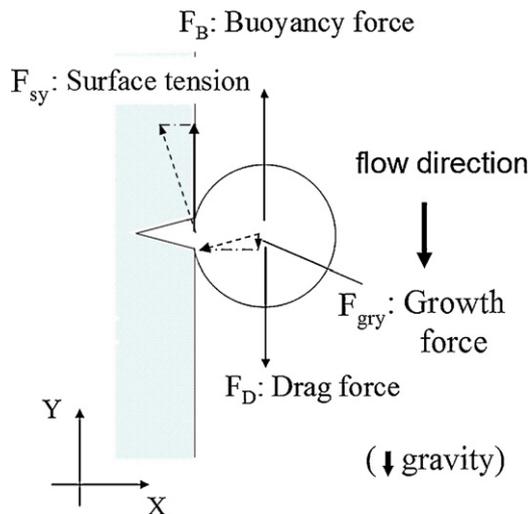
et al. (2004, 2005) where details of the mathematical expression are given.

2.3.2. Validation of bubble nucleation and detachment model

An experiment was performed using water and carbon dioxide in annular flow channel. The tendency of the solubility of the carbon dioxide with respect to the temperature change is opposite of the sodium, i.e., the solubility increases as the temperature. Therefore, a heater instead of the heat transfer tube is used to simulate the nucleation and the coolant flow direction is upward in the experiment. The average flow velocity is 505 mm/s and the gap width is 1 mm. As a result, the direction of the drag force is upward. With a high resolution CCD camera, the nucleation of bubbles and rising bubbles are recorded.

Experimental results are shown in Fig. 8 in which the bubble radius distributions are shown for the stationary bubbles on the heater and moving bubbles. It is seen that the radius of the stationary bubble is smaller in general than the moving bubbles. We assume that the crossing point of the two distribution curves corresponds to the bubble detachment radius, i.e., 105 μm.

From Eqs. (16) and (17) the movement of a bubble is calculated in inflow and crossflow directions and the detachment radius is evaluated. The bubble detachment radius differs by the vertical location because the temperature, solubility and pressure are different by the elevation. Table 1 shows the comparison of the calculation using the equations and the experimental result. Regarding the calculation, the minimum and maximum radii are shown. According to the model by Situ et al. (2004, 2005) that is
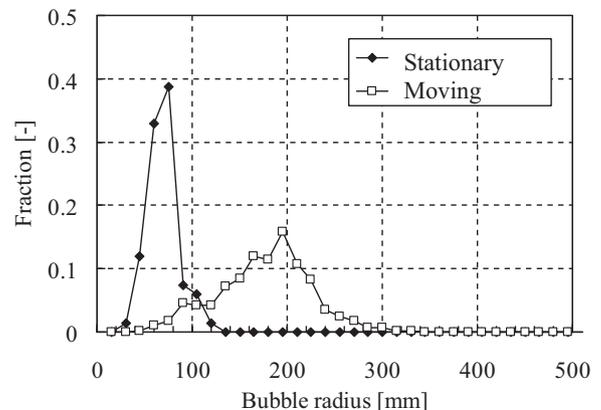

Fig. 6. Force balance in flow direction. Force balance in crossflow direction.

Fig. 8. Bubble radius distribution for stationary and moving bubbles.

Table 1
Comparison of experiment and computation for bubble emission.

	Bubble detachment radius [μm]	
Experiment	105	
Computation	99.5 (minimum)	101.4 (maximum)

employed in VIBUL code, it is calculated that the bubble nucleation takes place and it grows to 77–79 μm of radius to start the sliding in inflow direction on the wall surface with the flow. Then the bubble detaches in crossflow direction at the radius shown in Table 1. Comparing the model results and the experiment, the bubble detachment model by Situ et al. is in accordance with the experiment. It is considered that the comparison can be extrapolated to the reactor situations if the physical property for sodium is replaced with those of water. Therefore, the model is used in the VIBUL code.

3. Plant dynamics and bubble allowance level

3.1. Plant dynamics analysis and background bubbles

In the SFR design, the gas existence cannot be avoided. In addition, the gas entrainment is a concern in the smaller reactor vessel and larger velocity design than ever. Fig. 9 shows the modeling of the reactor vessel and the primary heat transport system of the JSFR. The argon gas bubble source is the gas entrainment in the upper plenum and the nucleation in the IHX. Helium gas bubble source is the control rods in the core and the nucleation in the IHX. Furthermore, mass exchange at the free surface in the upper plenum is considered.

Fig. 10 shows the argon and helium bubble radii distributions in the upper plenum computed by the VIBUL code with new models mentioned in Section 2. With regard to the gas source term, the
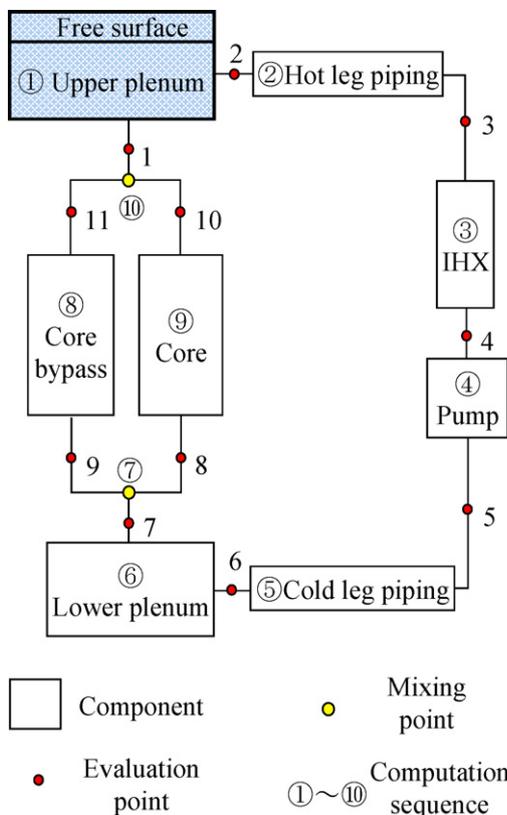
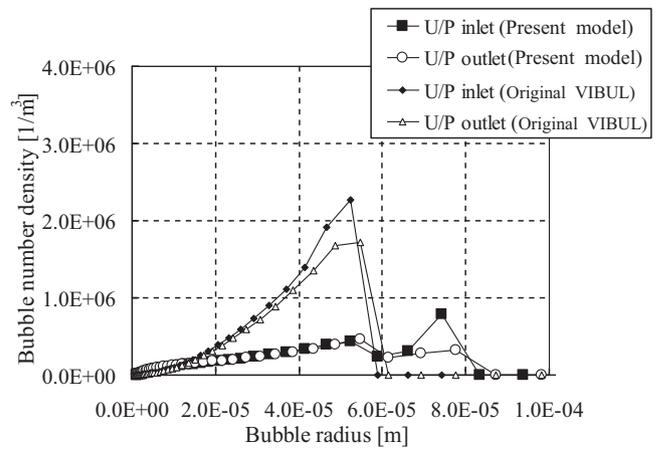

Fig. 9. SFR primary system.

Fig. 10. Gas bubble number density (argon and helium) in the upper plenum.

gas entrainment rate is assumed to be 4.0 cc/s with 50 μm diameter and the helium emission rate from the control rods are 0.4 cc/s with 50 μm diameter. The figure compares results from the original VIBUL code model and the present model. In the present model, we can see the distribution is more flattened and there are two peak values at 50 μm and 75 μm. The former comes from the gas entrainment at the free surface and the latter source is the nucleation at the IHX. The original VIBUL model tends to predict smaller bubble detachment radius that is nearly equal to the gas entrainment source.

On the basis of the VIBUL computation, we investigate the design guideline for the gas entrainment allowance level. Here we use the void fraction at the core inlet as the parameter of the design allowance level. If the gas bubbles pass the reactor core, it causes positive reactivity that is an important design consideration.

First of all, we compute the background level of the void fraction. If the gas entrainment at the free surface is neglected, the void fraction at the core inlet is 4.8×10^{-7}. It consists of 4.7×10^{-8} argon gas and 4.3×10^{-7} helium gas. We see the background of the argon gas is smaller than the helium gas by one order of magnitude. In the following, we consider the background void fraction level be 4.8×10^{-7}. From parametric computations, the core inlet void fraction increases in proportional to the entrainment amount as the gas entrainment rate increases.

Now let us consider the background void fraction. In the safety design of the JSFR, a requirement of gas entrainment rate should be prescribed. It is reasonable to set the requirement comparative to the background level. Fig. 11 shows the helium gas bubble number density. The first peak at 40 mm is the source term from the control
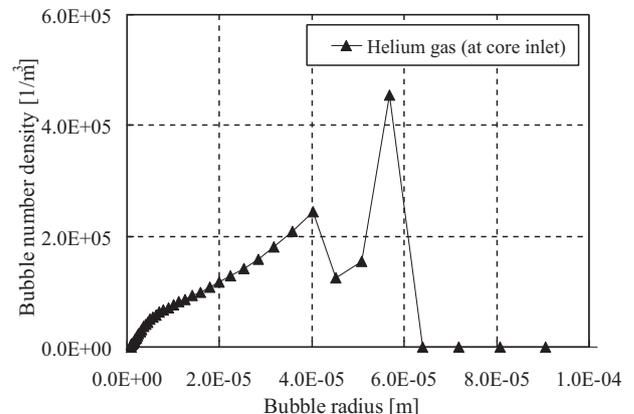

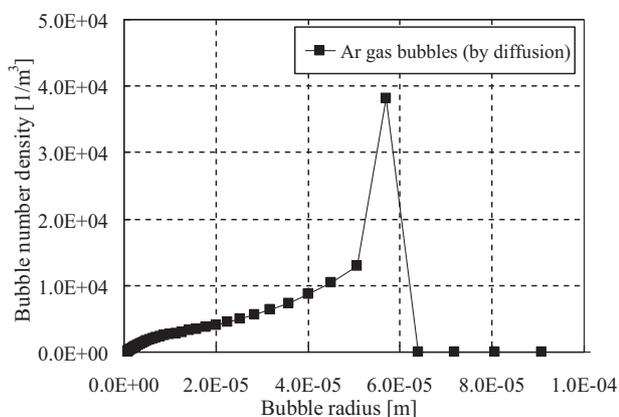**Fig. 11.** Helium bubble number density at the core inlet as a function of radius.

Fig. 12. Bubble number density at the core inlet for the argon gas with no gas entrainment.

Fig. 14. Void fraction at the core inlet as a function of the entrained bubble radius.

rods and the second peak at 60 mm is due to the nucleation. It is noted that the helium gas solubility is higher than argon by two orders of magnitude. Fig. 12 shows the bubble number density for the argon gas when the no gas entrainment is assumed. The argon gas source is the diffusion at the free surface, which appears at the IHX tube surface by the nucleation. Figs. 11 and 12 indicate what the background bubble number density for helium and argon gases is in the situation that the gas entrainment is completely excluded.

3.2. Plant dynamics analysis and background bubbles

The gas entrained rate and the entrained bubble size are uncertain while they are necessary information for the design guideline for the gas entrainment allowance level. Therefore the sensitivity of the parameters is investigated. Fig. 13 shows the void fraction at the core inlet when the entrained bubble radius varies. Gas entrainment rate is set to be constant, i.e., 4.0 cc/s. As the radius of the helium gas bubble emission rate is the same, the void fraction of the helium gas is constant and is 4.3×10^{-7}. It is seen that the total void fraction decreases as the entrained bubble radius.

In the following the tendency is investigated in detail. The gas bubbles at the core inlet is originated from one of three phenomena: (1) transport of the entrained gas bubbles at the free surface to the reactor core; (2) diffusion of the reactor cover gas to the sodium followed by bubble nucleation and detachment at the IHX; (3) dissolution of the entrained gas bubbles followed by bubble nucleation and detachment at the IHX.
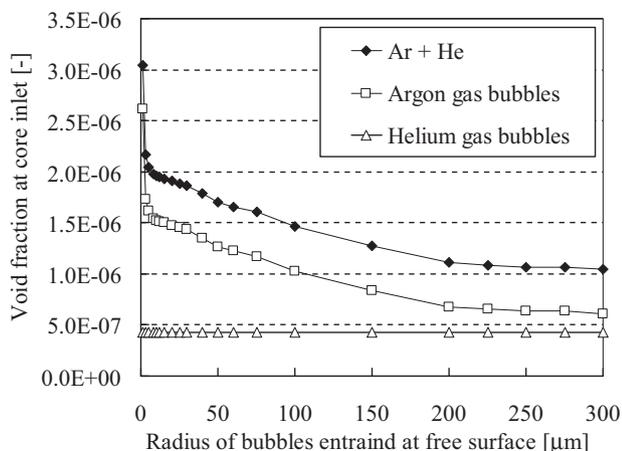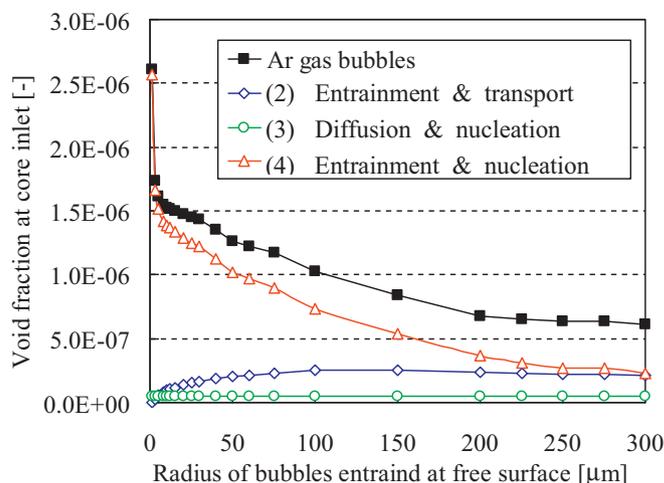
Contributions of the three phenomena are illustrated in Fig. 14. First of all, (1) entrainment and transport of the gas bubbles is shown by blue diamonds and (2) the diffusion and nucleation is shown by green circles. It is a matter of course that the diffusion effect is constant and does not depend on the entrained bubble radius. For small bubbles, the surface tension is large and most of the small bubbles are dissolved. The dissolved bubbles accordingly come out at the IHX. Therefore (3) the dissolution of the entrained bubbles and nucleation effect that is shown by red triangles is very important.

On the other hand, for larger bubble, the drag force becomes dominant and surface tension is relatively small. Therefore, the contribution of (1) the transport of entrained gas bubbles is more significant and the contribution of (3) the dissolution of the entrained gas and nucleation is not small. The two effects are almost competitive for bubbles with 250 μm radius or larger. Another important finding is that the void fraction is gradually decreasing as the bubble radius increases. It is explained by the fact that a large bubble for which buoyancy force is dominant is easily emitted from the free surface before carried to the outlet pipe nozzle. In summary, (3) the dissolution and nucleation is significant for small bubbles and contribution of (3) the dissolution and nucleation and (1) the direct transport of the babbles are comparative for large bubbles.

3.3. Design allowance level of gas entrainment

As discussed above, the void fraction at the core inlet is influenced by the entrained gas bubble radius and the entrainment rate. The relative importance of various phenomena such as diffusion, dissolution, transport, and nucleation and detachment varies depending on the bubble radius. The background level of the void fraction is 4.8×10^{-7}. Considering that the void fraction of 2.0×10^{-5} was evaluated to cause 0.013 cent of void reactivity, we can say the background value is small enough from the safety viewpoint. In the present discussion, we decide the design allowance level so that the void fraction at the core inlet is kept small enough comparing to the background level. Since the entrained bubble radius is unknown, two extreme cases are analyzed, i.e., the radii are 1 μm and 300 μm. The results are shown in Figs. 15 and 16, respectively in which the background level (4.8×10^{-7}) are subtracted in advance.

Fig. 15 shows the void fraction at the core inlet when the entrained bubble radius is 1 μm. The void fraction exceeds the background level if the entrained rate is greater than 0.75 cc/s. If we can limit the gas entrainment rate below 0.04 cc/s, the void fraction at
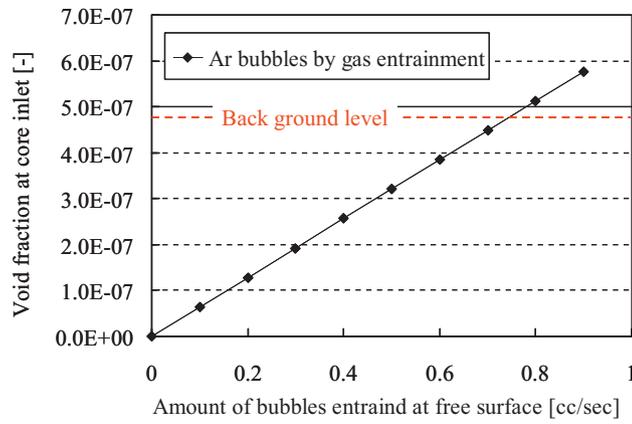

Fig. 13. Void fraction at the core inlet as a function of the entrained bubble radius.

Fig. 15. Void fraction at the core inlet as a function of the entrained bubble radius (entrained bubble radius is 1 μm).

Table 2
Comparison of sodium and water physical properties.

	Water	Liquid sodium
ρ: density (kg/m^3)	996.6	874
σ: surface tension (mN/m)	71.69	174

the core inlet falls below the 5% of the background level. Fig. 16 shows the results for the other extreme case where the entrained bubble radius is 300 μm. In this case, the void fraction exceeds the background level when the entrainment rate is 3.4 cc/s. From the safety viewpoint, smaller the entrained bubble radius assumption is more conservative.

The extremes of the bubble radius, i.e., 1 μm and 300 μm are justified as follows. The minimum radius of 1 μm is extremely small in comparison with an experimental evidence by Ezure et al. (2006) who observed the entrained bubble radius is 500–1500 μm with air and water experiment. Using the physical property of sodium and water as in Table 2 and the Weber number similarity, $We = 2r\rho\overline{u'^2}/\sigma$ a bubble in the sodium is equivalent to 2.5 times as large as in the water. In addition, it is noted here again that an assumption of gas entrainment of smaller radius bubbles gives conservative estimate. On the other hand, considering the bubble splitting radius (approximately 250 μm) in the region where the turbulent intensity is large such as a centrifugal pump, the maximum entrained gas radius of 300 μm may be justified regardless of Ezure's experiment.
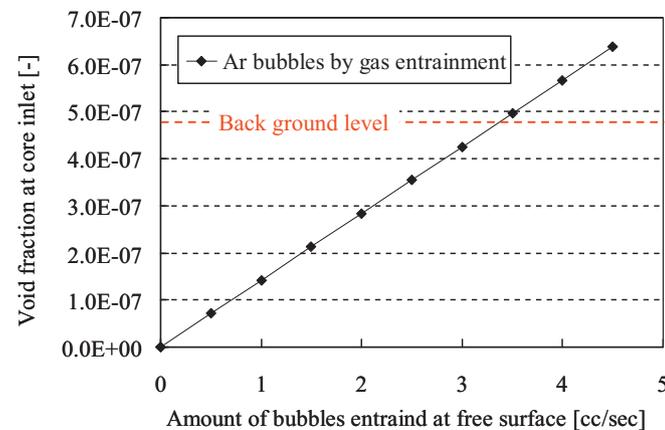

Fig. 16. Void fraction at the core inlet as a function of the entrained bubble radius (entrained bubble radius is 300 μm).
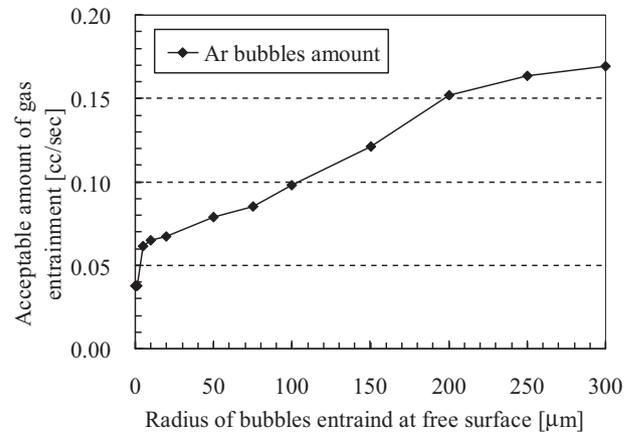

Fig. 17. Design map in terms of the entrainment rate and the entrained bubble radius.

If we assume the design allowance level of gas entrainment is that the core inlet void fraction is less than 5% of the background level, the design map in terms of the entrainment rate and the entrained bubble radius is shown in Fig. 17. This figure gives the allowance level of gas entrainment rate being given the entrained gas radius. It is noted that the allowance level is less restrictive for large bubbles.

Lastly, the authors consider the possibility of bubble removal by placing equipment that can separate bubbles from the sodium flow based on a case study. Assume the entrained gas bubble radius is 50 μm, from Fig. 17, we see the gas entrainment allowance level is 0.079 cc/s to keep the gas entrainment contribution less than 5% of the background level. We consider a situation where the gas entrainment rate is estimated to be 0.79 cc/s as the design condition, (ten times of the allowance level) and the allowance level is not achieved. Then, we determine to put a device in a location between the IHX and the reactor vessel to remove bubbles in the system. A question is what the required performance should be for the device. If the device can remove bubbles of its radius larger than r_0, the void fraction at the core inlet is evaluated as in Fig. 18 as a function of r_0. The void fraction allowance level is calculated as 5.0×10^{-7} (=4.8×10^{-7} time 1.05) and is shown in Fig. 18 if its increase is limited less than 5% of the background level. Consequently we obtain the design requirement for the device as it can remove bubbles with radius of 66 μm or larger to satisfy the allowance level of the gas entrainment rate.
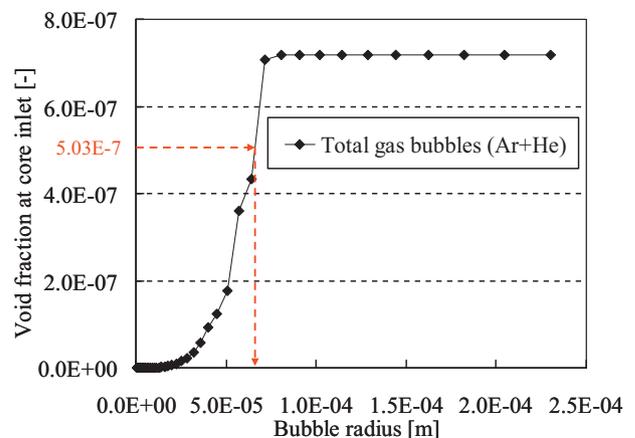

Fig. 18. Relationship of removed bubble radius and void fraction at core inlet.

4. Conclusions

In the present study, a gas entrainment allowance level at the free surface is discussed and rationalized for the JSFR design. First of all, the VIBUL code has been developed so that it can be applied to the JSFR design. As to the important phenomena, i.e., multi-dimensional flow effect in the plenum and the bubble nucleation and detachment in the IHX are studied in detail. The nucleation and detachment model is compared with the experimental data and the validity of the model is suggested.

Subsequently a computational model has been applied to evaluate the concentration distribution of the dissolved gas and the free gas bubble for steady state and transient conditions in the SFR system and the importance of the gas source has been evaluated. Using the plant dynamics code for the bubble behavior, the background level of the free gas (void fraction at the core inlet) has been obtained. As to the background level, the helium gas is the dominant contributor because of its high solubility. Assuming that the total void fraction should be kept below 105% of the background level, a preliminary design allowance level of gas entrainment is proposed as the map in terms of the entrainment rate and the entrained bubble radius. Furthermore, the possibility of bubble removal and design requirement of the device is investigated to satisfy the allowance level. It is noted that the background level is already very small in comparison with the induced void reactivity by the void passing the reactor core.

Future work is to reasonably establish the gas entrainment rate and the entrained gas bubble radius. In the JSFR design a dipped plate is installed below the free surface that can reduce the gas entrainment rate considerably. If we predict gas entrainment phenomena we have more flexibility in the design of the dipped plate for example, using the present design allowance level of gas entrainment. The entrained gas radius has been already measured with water (Ezure et al., 2006). Its applicability to the SFR conditions is to be established. From this viewpoint, a measurement of dissolved gas and free gas existence using a sodium loop will justify and validate the proposed design allowance level.

References

Berton, J.L., 1991. VIBUL, Un modèle de calcul de la vie des bulles en réacteur, NTCEA, SSAE, LSMI91, 023.
Clift, R., Grace, J.R., Weber, M.E., 1978. Bubbles, Drops and Particles. Academic Press.
Ezure, T., Kimura, N., 2006. Fundamental study on gas entrainment phenomenon. JAEA-Research 2006-067.
Ichimiya, M., Mizuno, T., Konomura, M., 2003. A promising sodium-cooled fast reactor concept and its R&D plan. In: Proc. of Global 2003 , New Orleans, LA.
Lewis, D.A., Davidson, J.F., 1982. Bubble splitting in shear flow. Trans. IChemE 60, 283–291.
Reed, E.L., Dropher, J.J., 1970. Solubility and diffusivity of inert gases in liquid sodium, potassium and NaK. Liquid Metal Engineering Center Report LMEC-69-36.
Situ, R., Hibiki, T., Ishii, M., et al., 2005. Bubble lift-off size in forced convection subcooled boiling flow. Int. J. Heat Mass Transfer 48, 5536–5548.
Situ, R., Mi, Y., Ishii, M., et al., 2004. Photographic study of bubble behaviors in forced convection subcooled boiling. Int. J. Heat Mass Transfer 47, 3659–3667.
Tatsumi, E., 2008. Development of Dynamics Model and Design Consideration of Gas Behavior in the Primary Coolant System of Sodium-Cooled Fast Reactor, Master Thesis, Osaka University, February (in Japanese).
Tatsumi, E., Takata, T., Yamaguchi, A., 2007. Modeling and quantification of nucleation, dissolution and transportation of bubbles in primary coolant system of sodium fast reactor. In: 15th International Conference on Nuclear Engineering, 10545.
Yamaguchi, A., Hashimoto, A., 2005. A computational model for dissolved gas and bubble behavior in the primary coolant system of sodium-cooled fast reactor. In: 11th International Topical Meeting on Nuclear Reactor Thermal-Hydraulics, 477.